Journal of Telecommunication, Electronic and Computer Engineering
ISSN: 2180 – 1843 e-ISSN: 2289-8131 Vol. 18 No. 1 (2026) 9-17
jtec.utem.edu.my
DOI: https://doi.org/10.54554/jtec.2026.18.01.002

Analysis of the Correspondence Between DCT and Non-Classical Walsh-Hadamard Transforms for Code-Controlled Steganography

Balandina Nataliia*, Trofymenko Olena, Yevdokymov Denys
National University "Odesa Law Academy", Fontanska road, 23, Odesa, 65009, Ukraine

Article Info

Article history:
Received Oct 23rd, 2025
Revised Mar 8th, 2026
Accepted Mar 27th, 2026
Published Mar 31st, 2026

Index Terms:
Discrete Mathematics
Walsh-Hadamard Transform
Discrete Cosine Transform
Hadamard Matrices

Abstract

In the modern digital environment, where vast amounts of multimedia data are continuously exchanged across global networks, ensuring secure and covert communication has become a critical challenge. Steganography plays a crucial role in this context by allowing the imperceptible embedding of secret information into digital media, including images, audio, and video signals. However, most state-of-the-art steganographic methods rely on computationally intensive mathematical transforms, including the Discrete Cosine Transform (DCT), Singular Value Decomposition, and various wavelet-based or deep-learning-based approaches. While these techniques achieve high robustness and embedding capacity, their high computational complexity limits practical implementation on resource-constrained platforms such as mobile devices, embedded systems, and Internet-of-Things environments. A promising direction for overcoming these limitations is the development of code-controlled steganographic methods, which operate directly in the spatial domain. Their efficiency is based on establishing deterministic relationships between DCT coefficients and those of the Walsh-Hadamard Transform (WHT), enabling precise code-based control of the embedding process. To date, such research has been limited to classical Sylvester-type Hadamard matrices. However, multiple non-equivalent classes of Hadamard matrices exist, and exploring their properties may unlock new opportunities for efficient and secure information embedding. This paper presents a comprehensive analysis of the correspondence between DCT coefficients and WHT coefficients derived from five non-equivalent classes of Hadamard matrices of order 16. Large-scale experimental research was performed using 530 images from the NRCS public database. Each image was processed in 16×16 blocks, with controlled perturbations applied to individual DCT coefficients. The resulting changes in WHT coefficients were analyzed to determine the mappings between the transform domains. The results reveal that while the classical Sylvester matrix preserves a one-to-one correspondence with DCT, non-classical Hadamard matrix constructions exhibit overlapping mappings, particularly in the high-frequency range. This overlap, although reducing spectral resolution, introduces beneficial redundancy for steganographic applications, enhancing robustness and resistance to steganalysis. The findings provide a foundation for developing high-performance, spatial-domain steganographic schemes that exploit the structural diversity of non-classical Hadamard matrices for improved efficiency and security.

This is an open access article under the CC BY-NC-ND 4.0 license.

*Corresponding Author: nataliabalandina2103@gmail.com

I. INTRODUCTION AND STATEMENT OF THE PROBLEM

Steganography plays a crucial role in today's world, where vast amounts of multimedia information are continuously exchanged across digital networks. With the exponential growth of image, video, and audio data, ensuring secure and covert communication has become increasingly important. Steganographic techniques enable information to be embedded within digital media in a manner that is imperceptible to human perception, thereby allowing for secure transmission without drawing attention. The development of robust methods for embedding and detecting hidden information is essential for maintaining privacy, data integrity, and security in digital communications [1].

Modern steganographic methods are expected to meet a range of demanding requirements. These include ensuring reliability of perception, providing sufficient bandwidth for covert data, maintaining robustness against steganalysis attacks, and achieving high computational efficiency. Performance is especially critical today, as many steganographic techniques are implemented on mobile

platforms, Internet-of-Things (IoT) devices, or embedded systems, where computational resources are limited and real-time processing is often required.

Today, a wide variety of steganographic methods have been developed that operate in the transform domain, including techniques based on the Discrete Cosine Transform (DCT), Singular Value Decomposition (SVD), and mathematical transformations. While these methods often demonstrate high effectiveness in terms of capacity and robustness, they typically require substantial computational resources. This high computational demand limits their applicability on resource-constrained platforms or in real-time scenarios, such as mobile devices, embedded systems, or IoT applications.

In particular, Durafe and Patidar [2] proposed a blind image steganography algorithm utilizing fractal images as cover media, combined with SVD and Integer Wavelet Transform (IWT) or Discrete Wavelet Transform (DWT). While effective in embedding capacity and robustness, the algorithm's reliance on IWT/DWT and SVD requires significant computational resources, making real-time or mobile implementations challenging.

Song et al. [3] introduced a JPEG steganography method based on DCT and SVD within the nonsubsampled shearlet transform domain. This approach enhances robustness against compression attacks but involves complex computations due to the shearlet transform and SVD, which can be computationally intensive. Pilania et al. [4] developed a Region of Interest (ROI)-based video steganography technique using SVD in the wavelet domain. While it offers improved robustness and capacity, the use of wavelet transforms and SVD increases the computational load, potentially hindering performance on resource-constrained devices.

In [5], Liu et al. proposed a robust JPEG image steganography method employing wavelet domain SVD and Adaptive Quantization Index Modulation (QIM). The integration of wavelet transforms and SVD, along with adaptive QIM, enhances robustness but also requires considerable computational power, limiting its applicability to devices with limited processing capabilities. In [6], Chaudhary et al. presented an image steganography approach based on spectral graph wavelets using SVD and the Arnold transform. The complexity of the method arises from the spectral graph wavelet transform and SVD, requiring substantial computational resources, which may not be feasible for real-time applications on low-power devices.

Mathivanan and Ganesh [7] introduced an ECG steganography scheme utilizing Tunable Q-factor Wavelet Transform (TQWT) and SVD. While effective for embedding ECG signals, the TQWT and SVD processes are computationally demanding, posing challenges for implementation on devices with limited processing power.

Ahmad et al. [8] proposed an enhanced CNN-DCT steganography method combining Convolutional Neural Networks (CNNs) and DCT. The deep learning aspect added significant computational overhead, making it less suitable for real-time applications on devices with limited resources.

In summary, while these steganographic techniques offer enhanced robustness and capacity, their reliance on complex transforms and decompositions often results in high computational demands. This makes them less suitable for real-time applications on resource-constrained platforms, highlighting the need for more efficient steganographic methods.

A significant breakthrough in the field of steganography is the development of a code-controlled steganographic method [9], which operates directly in the spatial domain. This approach achieves exceptionally high computational efficiency while outperforming existing methods in key performance metrics such as embedding capacity, perceptual transparency, and robustness. By leveraging code-based control mechanisms, the method enables precise manipulation of pixel values, ensuring secure and covert information embedding with minimal computational overhead.

The development of this high-performance steganographic method is made possible by the established relationship between the Walsh-Hadamard Transform (WHT) and the DCT [10]. Understanding this correspondence allows for the synthesis of codewords that serve as the basis for code-based control. Essentially, code-based control enables precise manipulation of the embedding process by mapping modifications in one transform domain to predictable changes in another. This mechanism ensures that the embedding can be guided deterministically, providing both high efficiency and robustness, while minimizing perceptual distortion and computational overhead.

The concept of code-controlled embedding has undergone significant development over the past decade. Early methods, such as the multi-level codewords approach proposed by Kobozeva and Sokolov [11], provided a framework for precise control of information embedding in digital signals. These methods allowed the embedding process to follow predetermined code structures, enhancing the reliability and interpretability of hidden information.

Subsequent studies focused on improving the efficiency of blind decoding, ensuring that embedded information could be reliably recovered even without the original container [12]. These improvements were critical for practical deployment in real-world scenarios, where the presence of the original container on the decoding side is challenging.

Further research addressed robustness against distortions and practical attacks. Zihinova and Sokolov [13] introduced enhancements to the original code-controlled embedding method to increase its resilience, while Sokolov et al. [14] proposed high-capacity spatial steganography schemes based on perfect binary arrays, demonstrating that structured code-controlled embeddings can support larger payloads without compromising imperceptibility.

Recent studies have emphasized security against statistical steganalysis. Lanovska and Sokolov [15] rigorously evaluated code-controlled embedding, showing that the method provides significant resistance to detection by modern steganalysis tools. These results confirm that careful design of code structures can simultaneously achieve high robustness and low detectability.

Nevertheless, all these results have been obtained using the classical Walsh-Hadamard Transform Sylvester construction. In contrast, non-classical constructions also exist, and exploring their properties opens up new possibilities. Investigating these alternative WHT matrices may reveal novel patterns of correspondence with DCT coefficients, potentially enabling more flexible and efficient codeword synthesis for code-based control in steganography.

The purpose of this paper is to investigate the relationship between DCT coefficients and both classical and non-

classical WHT matrices. By systematically analyzing how modifications in DCT coefficients affect the WHT domain, we aim to establish a mapping that enables the synthesis of codewords for code-based control in steganography. This research aims to establish a foundation for developing high-performance, spatial-domain steganographic methods that combine efficiency, robustness, and minimal perceptual distortion, while also exploring the new opportunities offered by non-classical WHT constructions.

Although the code-controlled steganographic method and the theoretical correspondence between the Discrete Cosine Transform and the Walsh-Hadamard Transform were previously established in [9] and [10], those studies were limited to the classical Sylvester construction of Hadamard matrices.

In contrast, the present paper extends this theoretical framework to non-classical Hadamard matrix constructions belonging to different equivalence classes. While classical Sylvester matrices provide a strict one-to-one correspondence between DCT and WHT coefficients, alternative Hadamard structures may exhibit fundamentally different mapping properties.

The novelty of this research lies in the systematic investigation of how different non-equivalent Hadamard matrix classes influence the correspondence between transform domains. Through large-scale experimental analysis, this study demonstrates that non-classical constructions introduce overlapping mappings, particularly in the high-frequency range. Although such overlap reduces spectral resolution, it creates structural redundancy that may enhance robustness and concealment in steganographic applications.

Thus, this paper does not merely extend previous results in scope but reveals new structural properties of non-classical Hadamard transforms that can be exploited in the design of code-controlled steganographic methods.

The main contributions of this work are summarized as follows:

1. A systematic analysis of the correspondence between DCT coefficients and WHT coefficients constructed from five non-equivalent classes of Hadamard matrices.
2. Large-scale experimental evaluation based on 530 images from a public dataset.
3. Identification of structural differences between classical Sylvester-type Hadamard matrices and non-classical constructions.
4. Demonstration that non-classical matrices introduce overlapping DCT-WHT mappings that may provide beneficial redundancy for steganographic embedding.

II. WHT MATRICES CONSTRUCTION

The Walsh-Hadamard transform is a widely used mathematical transform that decomposes signals or images into orthogonal Walsh functions, which take only binary values (+1 and –1). Due to its simplicity, orthogonality, and ability to concentrate energy, the WHT has found applications in diverse fields, including digital communications, error-correcting codes, image and video processing, pattern recognition, and steganography. Its importance lies in enabling efficient signal representation, fast computations, and precise control over modifications in the transform domain, making it an essential tool for both theoretical analysis and practical implementations. Let a digital image block be defined as X. Then, the Walsh-Hadamard Transform of this block is given by

$$W_X = H'_N X H'^T_N, \tag{1}$$

where $H'_N = \frac{1}{\sqrt{N}} H_N$, X is a matrix of size $N \times N$, and the Hadamard matrix H_N of order N is given by the Sylvester construction

$$H_{2^k} = \begin{bmatrix} H_{2^{k-1}} & H_{2^{k-1}} \\ H_{2^{k-1}} & -H_{2^{k-1}} \end{bmatrix}, \; H_1 = 1. \tag{2}$$

Sylvester matrices are square matrices of order 2^n, and their rows (or columns) are mutually orthogonal. This orthogonality ensures that the transform preserves energy and allows for efficient computation using fast Walsh-Hadamard Transform algorithms. The Sylvester construction has been extensively employed in steganography and coding because of its simplicity, regular structure, and favorable computational properties.

While previous papers have established the theoretical relationship between the Discrete Cosine Transform (DCT) and the classical Walsh-Hadamard Transform (WHT), it has been shown in [10] that a unique one-to-one mapping between these transforms does not generally exist. However, specific transformants exhibit a predominant correspondence.

In the present paper, this analysis is extended to non-classical Hadamard matrices. In these cases, the structure of the Hadamard matrix and the sequency ordering of its rows play a critical role in shaping the observed mapping between DCT and WHT coefficients. Due to the complexity of general analytical derivation, the theoretical considerations are complemented by an extensive empirical evaluation. This approach allows the identification of systematic correspondences that would be difficult to capture purely through formal proofs.

From a steganographic perspective, different equivalence classes of Hadamard matrices can exhibit distinct properties that directly impact the efficiency and effectiveness of code-based control methods. Although equivalent matrices preserve orthogonality and energy distribution, their specific row and column arrangements determine how modifications in the spatial domain propagate through the Walsh-Hadamard Transform. Consequently, some matrices may produce more concentrated or more evenly distributed changes in the transformed coefficients when a particular DCT coefficient is modified [16]. This variability can affect the embedding capacity, robustness to attacks, and perceptual transparency of the steganographic method. Exploring non-classical Hadamard matrices, therefore, provides an opportunity to optimize the mapping between spatial modifications and transformed-domain responses, potentially leading to more efficient and resilient steganographic schemes.

In this paper, representatives of the five equivalence classes of Hadamard matrices of order $N = 16$ are presented in Fig. 1 [17, 18]. These matrices illustrate the diversity of non-classical constructions beyond the classical Sylvester matrix, providing a foundation for investigating how different matrix structures influence the mapping between DCT coefficients and Walsh-Hadamard Transform coefficients.

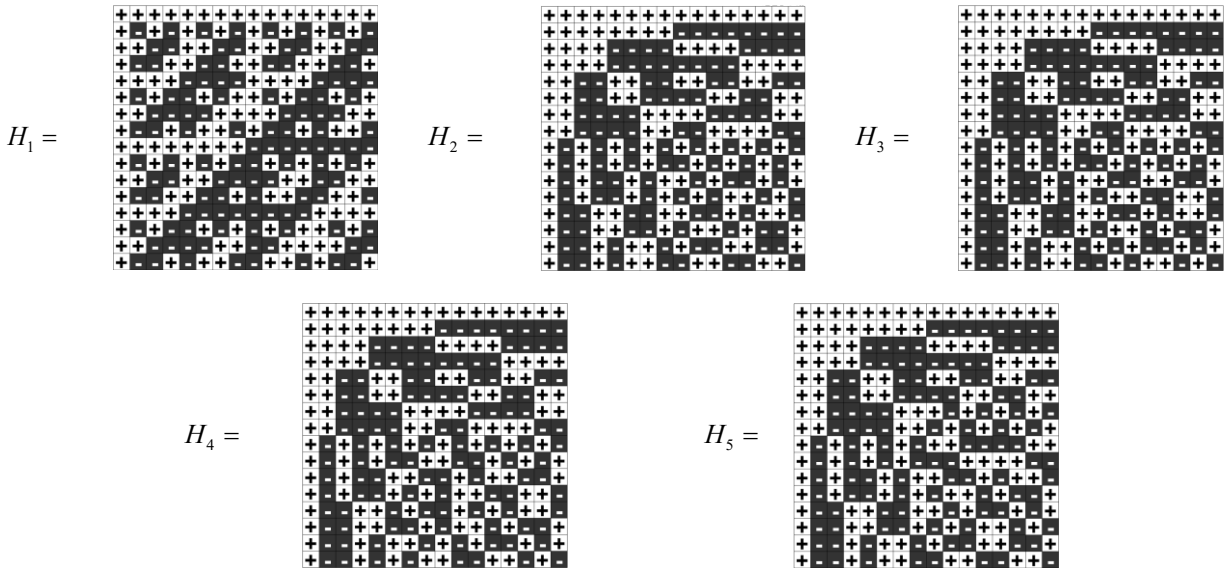


Figure 1. Representatives of equivalent classes of Hadamard matrices of order $N = 16$

III. RESEARCH ON THE SEQUENCY STRUCTURE OF EQUIVALENT CLASSES OF HADAMARD MATRICES

In the context of Walsh functions, each function, although not harmonic, can be characterized by a parameter known as sequency [19], which serves as an analogue of frequency for harmonic functions. For harmonic functions, sequency and frequency coincide, but for Walsh functions, sequency provides a discrete measure of the number of sign changes in a function over its domain. Formally, if the number of sign changes in a function over its interval is n_1, then its sequency s is defined as

$$s = \begin{cases} \frac{n_1}{2}, & \text{if } n_1 \text{ is even,} \\ \frac{n_1+1}{2}, & \text{if } n_1 \text{ is odd.} \end{cases}, \quad (3)$$

Researching the sequency of Hadamard matrices is important in applications such as steganography and signal processing because it characterizes how the variations of each function are distributed in time or space. Functions with lower sequency exhibit slower variations and are generally less sensitive to high-frequency modifications, while functions with higher sequency oscillate more rapidly. Understanding the sequency distribution of matrix rows allows one to predict the behavior of the WHT under various modifications and to optimize its use in code-controlled steganographic embedding.

In Table 1, the sequency values are presented for the rows of all five representatives of the equivalence classes of Hadamard matrices, as illustrated in Fig. 1. This allows for a direct comparison of the frequency-like characteristics of different matrix constructions and provides insight into how variations in matrix structure influence the distribution of sequencies across rows. Such an analysis is crucial for understanding the impact of non-classical Hadamard matrices on the mapping between spatial-domain modifications and their corresponding Walsh-Hadamard Transform responses in code-based steganography.

Table 1
Sequency values of rows for representatives of five equivalence classes of 16×16 Hadamard matrices

Row/ n_1, s		1	2	3	4	5	6	7	8	9	10	11	12	13	14	15	16
H_1	n_1	0	15	7	8	3	12	4	11	1	14	6	9	2	13	5	10
	s	0	8	4	4	2	6	2	6	1	7	3	5	1	7	3	5
H_2	n_1	0	1	3	2	7	6	4	5	15	14	12	13	9	10	10	9
	s	0	1	2	1	4	3	2	3	8	7	6	7	5	5	5	5
H_3	n_1	0	1	3	2	7	6	4	5	15	14	10	11	9	10	12	11
	s	0	1	2	1	4	3	2	3	8	7	5	6	5	5	6	6
H_4	n_1	0	1	3	2	7	6	4	5	15	12	10	11	11	10	12	11
	s	0	1	2	1	4	3	2	3	8	6	5	6	6	5	6	6
H_5	n_1	0	1	3	2	7	6	9	10	10	9	11	12	10	11	10	9
	s	0	1	2	1	4	3	5	5	5	5	6	6	5	6	5	5

In this research, the correspondence between the coefficients of the Discrete Cosine Transform and those of the Walsh-Hadamard Transform were analyzed based on all five non-equivalent classes of Hadamard matrices of order

$N = 16$ (Fig. 1). To ensure statistically reliable results, large-scale experiments were performed using a set of 530 images randomly selected from the NRCS public image database [20]. This dataset provides sufficient diversity in image content and structure to reveal meaningful patterns in the correspondence between DCT and non-classical WHT coefficients.

While the dataset does not cover all possible real-world scenarios, it was adequate for the theoretical and exploratory nature of this work. Future research may expand the analysis to additional datasets to further assess practical embedding performance based on the insights obtained here.

The experimental procedure consists of the following steps. Each image was first converted to grayscale (if originally in color) and then cropped so that its dimensions were multiples of 16, which allowed consistent block-based processing. Every image was divided into non-overlapping 16×16 pixel blocks, and both the DCT and WHT transforms were computed for each block.

To investigate the sensitivity and correspondence between the two domains, controlled perturbations were applied to the DCT coefficients. Specifically, for every block and for each of the $16\times16=256$ DCT coefficients, a small increment $\Delta=10$ was introduced to simulate localized modifications. After performing the inverse DCT to reconstruct the block, the WHT coefficients of the modified block were compared to those of the original block. The absolute differences were analyzed, and the Walsh-Hadamard coefficient most affected by the DCT perturbation was recorded.

This process was repeated across all blocks of all 530 images and for each of the five Hadamard matrix classes. The aggregated results produced detailed mappings between DCT and WHT coefficients. These mappings are summarized in Appendix, where correspondences are tabulated separately for each Hadamard matrix class.

The results demonstrate a clear distinction between the classical Sylvester-type Hadamard matrix H_1 and the four non-classical constructions $H_2 ... H_5$. For the Sylvester matrix, the mapping is strictly one-to-one: each DCT coefficient corresponds uniquely to a WHT coefficient. This ensures full preservation of spectral resolution and establishes a direct analogy between the two transforms.

In contrast, the non-classical Hadamard matrices reveal a different behavior. The mappings obtained for these structures contain multiple repetitions, meaning that several distinct DCT coefficients are associated with the same WHT coefficient. This phenomenon indicates that, although orthogonality is preserved, the frequency resolution in such transforms is effectively reduced. From the viewpoint of signal analysis, this introduces ambiguity and complicates the interpretation of spectral components.

Nevertheless, this characteristic should not be considered solely as a drawback. On the contrary, in the context of information hiding and steganography, such properties open new perspectives. The redundancy and overlapping of frequencies may be employed deliberately to mask embedded information and to increase resistance of the hidden data to statistical detection. In particular, the non-classical Hadamard structures provide alternative embedding domains that are less predictable and less directly correlated with standard frequency representations. This makes them attractive candidates for developing novel steganographic methods, where the very non-uniqueness of frequency mappings can be turned into an advantage by increasing uncertainty for an attacker.

Thus, the findings summarized in Appendix indicate while the Sylvester-type Hadamard matrix remains optimal for direct frequency-domain correspondences, the non-classical classes of Hadamard matrices demonstrate significant potential in steganographic applications due to their structural diversity and inherent capacity for frequency overlap.

A particularly important observation emerges from the experiments concerns the different behavior of low- and high-frequency coefficients. For low-frequency coefficients, the correspondence is highly stable across all five non-equivalent classes of Hadamard matrices. Whether the classical Sylvester construction or an alternative form is used, the mappings of low-order DCT coefficients converge to nearly identical Walsh-Hadamard positions. This can be explained by the fact that low-frequency components dominate the energy distribution within the image block, and their influence is robust to the specific ordering or symmetry of the Hadamard basis functions.

In contrast, the situation is markedly different from the high-frequency coefficients. These coefficients capture fine details, noise, and subtle local variations of intensity. In the classical Sylvester matrix, their mappings remain consistent and one-to-one, preserving the spectral locality of the transform. However, in the non-classical Hadamard matrices, the high-frequency contributions are dispersed across multiple Walsh-Hadamard positions, often leading to overlaps and redundancies. The experimental results provided in Appendix clearly demonstrate this dispersive behavior, where several distinct DCT coefficients converge into identical WHT indices in non-classical constructions.

From a practical standpoint, this divergence has a dual interpretation. For applications such as compression or spectral analysis, the dispersive nature of non-classical matrices may appear disadvantageous, as it reduces the distinctiveness of high-frequency components. However, in steganographic applications, the very same property becomes a strength. The scattering of high-frequency information across multiple transform coefficients introduces additional uncertainty into the spectral domain representation, complicating statistical detection and analysis of hidden data. Thus, the non-classical Hadamard matrices provide a promising alternative embedding domain that enhances robustness and secrecy by masking the footprints of information embedding within structurally ambiguous frequency mappings.

To further demonstration the relationship between individual DCT transformants and their impact on Walsh-Hadamard Transform representations, additional statistical experiments were performed using random image blocks. Square blocks of size 16×16 with uniformly distributed pixel intensities in the range $[0,255]$ were generated. For each block, the two-dimensional DCT was computed, and a single selected coefficient $S(u,v)$ was perturbed by adding a small offset Δ. The perturbed block was then reconstructed by applying the inverse DCT.

Both the original and perturbed blocks were subsequently transformed using five distinct Hadamard matrices (Fig. 1): the classical Walsh-Hadamard matrix and four non-classical Hadamard constructions. For each transformation, the absolute differences between the transform coefficients of the perturbed and original blocks were accumulated across a

large number of random trials (5000 blocks). The resulting averaged difference maps provided heatmaps that characterize the distribution of perturbation effects for a given DCT coefficient (Fig 2).

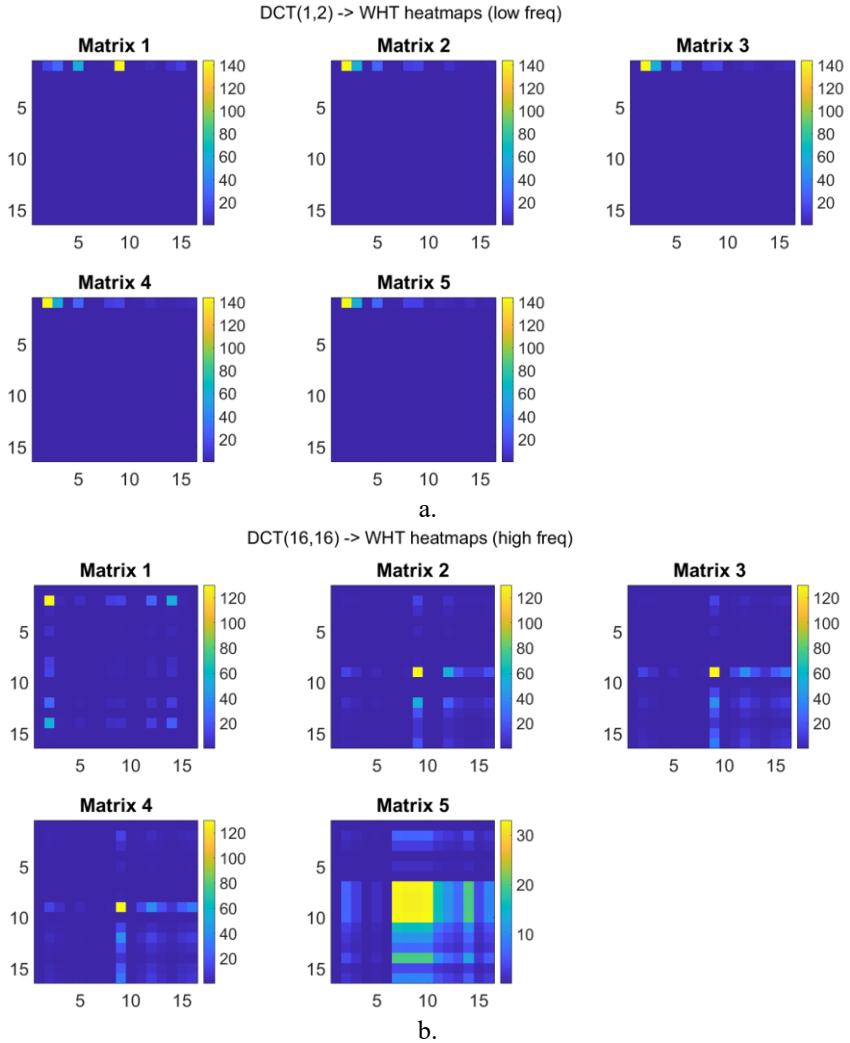


Figure 2. The difference heatmaps of the changes in Walsh-Hadamard transformants under the influence of perturbation of DCT transformant: a. – (1,2); b. – (16,16)

The heatmaps demonstrate that low-frequency perturbations remain concentrated within the low- and mid-frequency bands, while high-frequency perturbations are dispersed, especially in non-classical constructions. This indicates that the low-frequency content preserves its stability and energy localization, almost independently of the particular Hadamard construction used.

In contrast, perturbations of the high-frequency DCT transformation reveal notable differences. For the classical Hadamard matrix, the effect remains relatively concentrated, whereas for the non-classical constructions, the perturbation energy is spread more diffusely across the transform coefficients. Among them, the fifth Hadamard construction shows the most pronounced dispersion effect, with perturbations being distributed across a wide range of Walsh-Hadamard coefficients.

These results highlight that while low-frequency behavior is robust across different Hadamard realizations, the choice of non-classical Hadamard matrices significantly influences the propagation of high-frequency information. Such dispersion may be advantageous in applications requiring stronger mixing of spectral components, such as data hiding or information security.

IV. PRACTICAL IMPLICATIONS FOR STEGANOGRAPHY

Although the present work focuses on the structural correspondence between DCT and WHT domains, the results have direct implications for practical steganographic systems based on code-controlled embedding. In the classical Sylvester construction, the one-to-one mapping between DCT and WHT coefficients provides precise spectral control but also creates a predictable relationship between spatial modifications and transform-domain behavior, which may simplify statistical steganalysis.

In contrast, the non-classical Hadamard matrices analyzed here introduce overlapping mappings between DCT and WHT coefficients. This behavior increases uncertainty in the spectral representation of embedded modifications by distributing perturbations across multiple transform components, thereby potentially reducing detectability and improving robustness against statistical steganalysis.

The mappings established in this study provide a theoretical foundation for constructing future code-controlled embedding algorithms. While modern embedding methods achieve high efficiency, they often lack interpretability and

explicit spectral control. In contrast, the insights from this analysis offer structure-aware guidance that can enhance robustness and reduce detectability in practical steganographic systems.

Finally, a full evaluation of steganographic performance metrics, such as payload capacity, distortion measures (e.g., PSNR), and detectability using modern steganalysis techniques, remains an important direction for future research. This study situates the theoretical results within the broader field, highlighting their relevance to both classical transform-based approaches and contemporary deep-learning-based embedding schemes.

V. CONCLUSIONS

This paper provides a comprehensive analysis of the correspondence between the Discrete Cosine Transform and the Walsh-Hadamard Transform constructed using five non-equivalent classes of Hadamard matrices of order $N = 16$. The experimental results, obtained from large-scale testing on a diverse image dataset, reveal fundamental distinctions between the classical Sylvester-type matrix and alternative non-classical constructions.

It has been demonstrated that the classical Hadamard matrix preserves a strict one-to-one correspondence between DCT and WHT coefficients, ensuring full spectral resolution and predictable transform behavior. In contrast, non-classical Hadamard matrices exhibit overlapping mappings, where multiple DCT coefficients correspond to the same WHT coefficient. While this overlap reduces spectral distinctiveness, it introduces beneficial redundancy that can be strategically exploited in steganographic applications.

A key finding is that low-frequency coefficients maintain stable mappings across all Hadamard classes, reflecting consistent structural properties. Meanwhile, high-frequency coefficients demonstrate dispersive behavior under non-classical constructions, distributing perturbation energy across multiple transform components. This phenomenon can enhance the concealment of embedded data, improve resistance to statistical detection, and increase robustness against steganalysis.

From a broader perspective, the results confirm that non-classical Hadamard matrices offer new degrees of freedom for designing code-controlled embedding mechanisms. Their structural diversity allows for the synthesis of novel codewords and embedding strategies that combine high computational efficiency, strong security, and minimal perceptual distortion.

Thus, the research provides a solid theoretical and experimental foundation for the next generation of spatial-domain steganographic methods, leveraging advanced tools of linear algebra and spectral analysis. Future research will focus on developing practical embedding algorithms based on the identified mappings and assessing their performance in real-world scenarios, including mobile and IoT platforms.

APPENDIX

The correspondence between perturbation in DCT transformants and the most affected Walsh-Hadamard transformants

Matrix H_1

1,1	1,16	1,8	1,9	1,4	1,13	1,5	1,12	1,2	1,15	1,7	1,10	1,3	1,14	1,6	1,11
16,1	16,16	16,8	16,9	16,4	16,13	16,5	16,12	16,2	16,15	16,7	16,10	16,3	16,14	16,6	16,11
8,1	8,16	8,8	8,9	8,4	8,13	8,5	8,12	8,2	8,15	8,7	8,10	8,3	8,14	8,6	8,11
9,1	9,16	9,8	9,9	9,4	9,13	9,5	9,12	9,2	9,15	9,7	9,10	9,3	9,14	9,6	9,11
4,1	4,16	4,8	4,9	4,4	4,13	4,5	4,12	4,2	4,15	4,7	4,10	4,3	4,14	4,6	4,11
13,1	13,16	13,8	13,9	13,4	13,13	13,5	13,12	13,2	13,15	13,7	13,10	13,3	13,14	13,6	13,11
5,1	5,16	5,8	5,9	5,4	5,13	5,5	5,12	5,2	5,15	5,7	5,10	5,3	5,14	5,6	5,11
12,1	12,16	12,8	12,9	12,4	12,13	12,5	12,12	12,2	12,15	12,7	12,10	12,3	12,14	12,6	12,11
2,1	2,16	2,8	2,9	2,4	2,13	2,5	2,12	2,2	2,15	2,7	2,10	2,3	2,14	2,6	2,11
15,1	15,16	15,8	15,9	15,4	15,13	15,5	15,12	15,2	15,15	15,7	15,10	15,3	15,14	15,6	15,11
7,1	7,16	7,8	7,9	7,4	7,13	7,5	7,12	7,2	7,15	7,7	7,10	7,3	7,14	7,6	7,11
10,1	10,16	10,8	10,9	10,4	10,13	10,5	10,12	10,2	10,15	10,7	10,10	10,3	10,14	10,6	10,11
3,1	3,16	3,8	3,9	3,4	3,13	3,5	3,12	3, 2	3,15	3,7	3,10	3,3	3,14	3,6	3,11
14,1	14,16	14,8	14,9	14,4	14,13	14,5	14,12	14,2	14,15	14,7	14,10	14,3	14,14	14,6	14,11
6,1	6,16	6,8	6,9	6,4	6,13	6,5	6,12	6, 2	6,15	6,7	6,10	6,3	6,14	6,6	6,11
11,1	11,16	11,8	11,9	11,4	11,13	11,5	11,12	11,2	11,15	11,7	11,10	11,3	11,14	11,6	11,11

Matrix H_2

1,1	1,2	1,4	1,3	1,8	1,7	1,5	1,6	1,16	1,15	1,13	1,14	1,9	1,12	1,12	1,9
2,1	2,2	2,4	2,3	2,8	2,7	2,5	2,6	2,16	2,15	2,13	2,14	2,9	2,12	2,12	2,9
4,1	4,2	4,4	4,3	4,8	4,7	4,5	4,6	4,16	4,15	4,13	4,14	4,9	4,12	4,12	4,9
3,1	3,2	3,4	3,3	3,8	3,7	3,5	3,6	3,16	3,15	3,13	3,14	3,9	3,12	3,12	3,9
8,1	8,2	8,4	8,3	8,8	8,7	8,5	8,6	8,16	8,15	8,13	8,14	10,9	8,12	10,12	10,9
7,1	7,2	7,4	7,3	7,8	7,7	7,5	7,6	7,16	7,15	7,13	7,14	7,9	11,12	7,12	11,9
5,1	5,2	5,4	5,3	5,8	5,7	5,5	5,6	5,16	5,15	5,13	5,14	5,9	5,12	5,12	5,9
6,1	6,2	6,4	6,3	6,8	6,7	6,5	6,6	6,16	6,15	6,13	6,14	6, 9	6,12	6,12	6,9
16,1	16,2	16,4	16,3	16,8	16,7	16,5	16,6	16,16	16,15	16,13	16,14	16,9	16,12	16,12	16,9
15,1	15,2	15,4	15,3	15,8	15,7	15,5	15,6	15,16	15,15	15,13	15,14	15,9	15,12	15,12	15,9
13,1	13,2	13,4	13,3	13,8	13,7	13,5	13,6	13,16	13,15	13,13	13,14	13,9	13,12	13,12	13,9
14,1	14,2	14,4	14,3	14,8	14,7	14,5	14,6	14,16	14,15	14,13	14,14	14,9	14,12	14,12	14,9
9,1	9,2	9,4	9,3	9,8	9,11	9,5	9,6	9,16	9,15	9,13	9,14	9,9	9,12	9,12	9, 9
12,1	12,2	12,4	12,3	12,10	12,7	12,5	12,6	12,16	12,15	12,13	12,14	12,9	12,12	12,12	12,9
12,1	12,2	12,4	12,3	12,8	12,11	12,5	12,6	12,16	12,15	12,13	12,14	12,9	12,12	12,12	12,9

9,1	9,2	9,4	9,3	9,10	9,7	9,5	9,6	9,16	9,15	9,13	9,14	9,9	9,12	9,12	9,9

Matrix H_3

1,1	1,2	1,4	1,3	1,8	1,7	1,5	1,6	1,16	1,15	1,9	1,13	1,9	1,9	1,14	1,12
2,1	2,2	2,4	2,3	2,8	2,7	2,5	2,6	2,16	2,15	2,9	2,13	2,9	2,9	2,14	2,12
4,1	4,2	4,4	4,3	4,8	4,7	4,5	4,6	4,16	4,15	4,9	4,13	4,9	4,9	4,14	4,12
3,1	3,2	3,4	3,3	3,8	3,7	3,5	3,6	3,16	3,15	3,9	3,13	3,9	3,9	3,14	3,12
8,1	8,2	8,4	8,3	8,8	8,7	8,5	8,6	8,16	8,15	8,9	8,13	10,9	10,9	8,14	8,12
7,1	7,2	7,4	7,3	7,8	7,7	7,5	7,6	7,16	7,15	7,13	11,13	7,9	11,9	7,14	7,12
5,1	5,2	5,4	5,3	5,8	5,7	5,5	5,6	5,16	5,15	5,9	5,13	5,9	5,9	5,14	5,12
6,1	6,2	6,4	6,3	6,8	6,7	6,5	6,6	6,16	6,15	6,9	6,13	6,9	6,9	6,14	6,12
16,1	16,2	16,4	16,3	16,8	16,7	16,5	16,6	16,16	16,15	16,9	16,13	16,9	16,9	16,14	16,12
15,1	15,2	15,4	15,3	15,8	15,7	15,5	15,6	15,16	15,15	15,9	15,13	15,9	15,9	15,14	15,12
9,1	9,2	13,4	9,3	9,8	9,11	13,5	9,6	9,16	13,15	9,9	9,13	13,9	13,9	9,14	9,12
13,1	13,2	9,4	9,3	13,8	9,7	13,5	13,6	13,16	9,15	9,13	13,13	13,9	13,9	13,14	13,12
9,1	9,2	9,4	9,3	9,10	9,7	9,5	9,6	9,16	9,15	9,13	9,13	9,9	9,9	9,14	9,12
9,1	9,2	9,4	9,3	9,10	9,7	9,5	9,6	9,16	9,15	9,13	9,13	9,9	9,9	9,14	9,12
14,1	14,2	14,4	14,3	14,8	14,7	14,5	14,6	14,16	14,15	14,9	14,13	14,9	14,9	14,14	14,12
12,1	12,2	12,4	12,3	12,8	12,7	12,5	12,6	12,16	12,15	12,9	12,13	12,9	12,9	12,14	12,12

Matrix H_4

1,1	1,2	1,4	1,3	1,8	1,7	1,5	1,6	1,16	1,15	1,11	1,13	1,13	1,9	1,14	1,12
2,1	2,2	2,4	2,3	2,8	2,7	2,5	2,6	2,16	2,15	2,11	2,13	2,13	2,9	2,14	2,12
4,1	4,2	4,4	4,3	4,8	4,7	4,5	4,6	4,16	4,15	4,11	4,13	4,13	4,9	4,14	4,12
3,1	3,2	3,4	3,3	3,8	3,7	3,5	3,6	3,16	3,15	3,11	3,13	3,13	3,9	3,14	3,12
8,1	8,2	8,4	8,3	8,8	8,7	8,5	8,6	8,16	8,15	8,11	10,13	10,13	8,9	8,14	8,12
7,1	7,2	7,4	7,3	7,8	7,7	7,5	7,6	7,16	7,15	7,11	7,9	7,13	7,9	7,14	7,12
5,1	5,2	5,4	5,3	5,8	5,7	5,5	5,6	5,16	5,15	5,11	5,13	5,13	5,9	5,14	5,12
6,1	6,2	6,4	6,3	6,8	6,7	6,5	6,6	6,16	6,15	6,11	6,13	6,13	6,9	6,14	6,12
16,1	16,2	16,4	16,3	16,8	16,7	16,5	16,6	16,16	16,15	16,11	16,13	16,13	16,9	16,14	16,12
15,1	15,2	15,4	15,3	15,8	15,7	15,5	15,6	15,16	15,15	15,11	15,13	15,13	15,9	15,14	15,12
11,1	11,2	11,4	11,3	11,8	11,7	11,5	11,6	11,16	11,15	11,11	11,13	11,13	11,9	11,14	11,12
13,1	13,2	9,4	9,3	13,8	9,7	9,5	13,6	13,16	9,15	9,11	9,13	9,13	13,9	13,14	13,12
13,1	13,2	13,4	13,3	13,8	13,7	13,5	13,6	13,16	13,15	13,11	13,13	13,13	13,9	13,14	13,12
9,1	9,2	9,4	9,3	9,10	9,7	9,5	9,6	9,16	9,15	9,11	9,13	9,13	9,9	9,14	9,12
14,1	14,2	14,4	14,3	14,8	14,7	14,5	14,6	14,16	14,15	14,11	14,13	14,13	14,9	14,14	14,12
12,1	12,2	12,4	12,3	12,8	12,7	12,5	12,6	12,16	12,15	12,11	12,13	12,13	12,9	12,14	12,12

Matrix H_5

1,1	1,2	1,4	1,3	1,8	1,7	1,16	1,15	1,15	1,16	1,12	1,14	1,9	1,13	1,9	1,9
2,1	2,2	2,4	2,3	2,8	2,7	2,16	2,15	2,5	2,16	2,12	2,14	2,9	2,13	2,9	2,9
4,1	4,2	4,4	4,3	4,8	4,7	4,16	4,15	4,15	6,16	4,12	4,14	6,9	4,13	4,9	4,9
3,1	3,2	3,4	3,3	3,8	3,7	3,5	3,15	3,5	3,16	3,12	3,14	3,9	3,13	3,9	3,9
8,1	8,2	8,4	8,3	8,8	8,7	8,16	8,15	10,15	10,16	8,12	8,14	8,9	10,9	8,9	10,9
7,1	7,2	7,4	7,3	7,8	7,7	11,16	7,5	11,15	7,16	7,12	7,14	7,9	11,9	7,9	11,9
16,1	16,2	16,6	5,3	16,10	15,7	15,5	16,5	16,5	16,16	16,12	16,14	5,9	16,13	16,9	16,9
15,1	15,2	15,4	5,3	15,8	5,7	15,16	5,5	5,15	5,16	15,12	5,14	15,9	15,9	15,9	15,9
5,1	5,2	5,4	15,3	15,8	5,11	15,15	15,15	15,15	5,16	5,12	5,14	5,9	5,13	5,9	5,9
16,1	16,2	16,4	16,3	16,8	16,7	16,5	16,15	16,15	16,16	16,13	16,14	16,9	16,13	16,9	16,9
12,1	12,2	12,4	12,3	12,8	12,7	12,16	12,5	12,15	12,16	12,12	12,14	12,9	12,13	12,9	12,9
14,1	14,2	14,4	14,3	14,8	14,7	14,16	14,5	14,15	14,16	14,12	14,14	14,9	14,13	14,9	14,9
9,1	9,2	9,6	9,3	9,8	9,11	9,16	13,15	9,15	13,16	9,12	9,14	9,9	9,13	13,9	13,9
13,1	13,2	9,4	9,3	9,10	9,7	13,16	13,15	9,15	13,16	13,12	9,14	13,13	9,13	13,9	13,9
9,1	9,2	9,4	9,3	9,10	9,7	9,16	9,5	9,15	9,16	9,12	9,14	9,13	9,13	9,9	9,9
9,1	9,2	9,4	9,3	9,10	9,7	9,16	9,5	9,15	9,16	9,12	9,14	9,13	9,13	9,9	9, 9

CONFLICT OF INTEREST

The authors declare that there is no conflict of interest regarding the publication of the paper.

AUTHOR CONTRIBUTION

All authors contributed significantly to the development of this paper.

Conceptualization and methodology: Nataliia Balandina, Olena Trofymenko, Denys Yevdokymov.

Software, data curation, and experimentation: Olena Trofymenko, Denys Yevdokymov.

Formal analysis and validation: Nataliia Balandina, Denys Yevdokymov.

Writing and original draft preparation: Nataliia Balandina.

Writing, review, and editing: Nataliia Balandina, Olena Trofymenko, Denys Yevdokymov.

All authors have read and approved the final manuscript and agree to be accountable for all aspects of the paper.

REFERENCES

[1] D. R. A. Bashir, "The role of steganography, blockchain and advanced techniques", Blockchain Beyond Borders: Ethical Challenges and Regulatory Solutions, pp. 312, 2025.

[2] A. Durafe, V. Patidar, "Development and analysis of IWT-SVD and DWT-SVD steganography using fractal cover", Journal of King Saud University-Computer and Information Sciences, vol. 34, no. 7, pp. 4483-4498, 2022.

[3] X. Song et al., "Robust JPEG steganography based on DCT and SVD in nonsubsampled shearlet transform domain", Multimedia Tools and Applications, vol. 81, no. 25, pp. 36453-36472, 2022.

[4] U. Pilania, R. Tanwar, P. Gupta, "An ROI-based robust video steganography technique using SVD in wavelet domain", Open Computer Science, vol. 12, no. 1, pp. 1-16, 2022.

[5] J. Liu et al., "Robust JPEG image steganography using wavelet domain SVD and adaptive QIM" in Proc. of 8th International Conference on Signal and Image Processing (ICSIP), IEEE, 2023, pp. 434-438.

[6] S. Chaudhary, S. Hiranwal, C. P. Gupta, "Spectral Graph Wavelet Based Image Steganography Using SVD and Arnold Transform", Traitement du Signal, vol. 38, no. 4, pp. 1113-1121, 2021.

[7] P. Mathivanan, A. Balaji Ganesh, "ECG steganography based on tunable Q-factor wavelet transform and singular value decomposition", International Journal of Imaging Systems and Technology, vol. 31, no. 1, pp. 270-287, 2021.

[8] S. Ahmad et al., "Enhanced CNN-DCT steganography: Deep learning-based image steganography over cloud", SN Computer Science, vol. 5, no. 4, pp. 408, 2024.

[9] A.A. Kobozeva, A.V. Sokolov, "Robust Steganographic Method with Code-Controlled Information Embedding", Problemele energeticii regionale, no. 4 (52), pp. 115-130, 2021.

[10] A.A. Kobozeva, A.V. Sokolov, "Theoretical foundations for constructing effective codewords for the code-controlled information embedding steganographic method", Radiotekhnika, 4(207), pp. 27-39, 2021.

[11] A.A. Kobozeva, A.V. Sokolov, "Steganographic Method with Code Control of Information Embedding Based on Multi-level Code Words", Radioelectronics and Communications Systems, 66, (4), pp. 173-189, 2023. doi: 10.3103/S0735272723040052

[12] A.V. Sokolov, O.O. Ihnatenko, N.M. Balandina, "Increasing the Efficiency of Blind Decoding of the Steganographic Method with Code Control of Additional Information Embedding", Problems of regional energetics, 62(2), pp. 121-137, 2024.

[13] Y. Zihinova, A. Sokolov, "Improvement of the steganographic method with code control to increase its robustness", Informatics and mathimatial methods in simulation, 4, pp. 314-323, 2024.

[14] A. Sokolov, D. Yevdokymov, O. Fraze-Frazenko, "High-Capacity Spatial Steganography Based on Perfect Binary Arrays", Proceedings of the Workshop on Scientific and Practical Issues of Cybersecurity and Information Technology, V International scientific and practical conference Information security and information technology (ISecIT 2025), Lutsk, Ukraine, June 9-11, pp. 187-196, 2025.

[15] O.O. Lanovska, A.V. Sokolov, "Steganalysis of a method with code-controlled information embedding in the Walsh-Hadamard transform domain", Informatics and mathematical methods in simulation, 14(4), pp. 273-283, 2024.

[16] M.I. Mazurkov, A.V. Sokolov, N.A. Barabanov, "On the effect of the type of orthogonal transform on PAPR of signal spectrum in CDMA systems", Informatics and Mathematical Methods in Simulation, Vol. 5, no. 1, pp. 28-37, 2015.

[17] M. Jr. Hall, "Hadamard matrices of order 16. Research Summary No. 36-10", Volume I, Jet Propulsion Laboratory, Pasadena, pp. 21-26, 1961.

[18] S. Steinerberger, "A note on approximate Hadamard matrices", Designs, Codes and Cryptography, 92(10), pp. 3125-3131, 2024.

[19] A.V. Bazhenov, "Digital Methods for Implementing Spatio-Temporal Signal Processing in Aviation Electronic Systems", SVVAIU, 2006. 219 p.

[20] Natural Resources Conservation Service (NRCS). United States Department of Agriculture. Accessed: Oct. 19, 2025, [Online.] Available: https://www.nrcs.usda.gov